

BINARY AND MULTIPLE STAR FORMATION IN MAGNETIC CLOUDS: BAR GROWTH AND FRAGMENTATION

FUMITAKA NAKAMURA

Faculty of Education and Human Sciences, Niigata University, 8050 Ikarashi-2, Niigata 950-2181, Japan;
 fnakamur@ed.niigata-u.ac.jp

AND

ZHI-YUN LI

Department of Astronomy, University of Virginia, P.O. Box 3818, Charlottesville, VA 22903;
 zl4h@virginia.edu

Draft version April 4, 2018

ABSTRACT

In the standard scenario of isolated low-mass star formation, strongly magnetized molecular clouds are envisioned to condense gradually into dense cores, driven by ambipolar diffusion. Once the cores become magnetically supercritical, they collapse to form stars. Previous studies based on this scenario are limited to axisymmetric calculations leading to single supercritical core formation. The assumption of axisymmetry has precluded a detailed investigation of cloud fragmentation, generally thought to be a necessary step in the formation of binary and multiple stars. In a series of papers, we studied the non-axisymmetric evolution of initially magnetically subcritical clouds, using a two-dimensional magnetohydrodynamic code based on the physically motivated thin-disk approximation. We found that such clouds become unstable to non-axisymmetric perturbations after the supercritical cores are formed due to ambipolar diffusion. In this paper, we focus on the evolution of clouds perturbed by an $m = 2$ mode of a modest fractional amplitude of 5%, with an eye on binary and multiple star formation. We show that for a wide range of initial cloud parameters, the $m = 2$ mode grows nonlinearly into a bar during the isothermal collapse after the supercritical core formation. The instability is driven by the domination of the magnetically-diluted gravity over the combined thermal and magnetic pressure gradient in the supercritical cores. Such gravity-dominated cores can break up into fragments during or after the isothermal phase of cloud evolution.

The outcome of fragmentation depends on the initial cloud conditions, such as the magnetic field strength, rotation rate, amount of cloud mass (relative to thermal Jeans mass) and mass distribution. It is classified into three different types: (1) *separate core formation*, in which the bar ($m = 2$) mode breaks up into two separate cores during the isothermal collapse, with a core separation of order 10^4 AU, (2) *bar fragmentation*, in which the $m = 2$ mode evolves into a needle-like, opaque “first bar” (at a density $n \gtrsim 10^{12} \text{ cm}^{-3}$), which breaks up into multiple fragments with initial masses of order $10^{-2} M_{\odot}$ and separations of order 10^2 - 10^3 AU, and (3) *disk fragmentation*, in which the bar growth remains slow during the isothermal collapse and the central region evolves into a rapidly rotating, opaque “first disk”, which breaks up into several self-gravitating blobs with separations less than the disk size ($\lesssim 10^2$ AU). These three types of fragmentation loosely correspond to the empirical classification of embedded binary and multiple systems of Looney, Mundy, & Welch, based on millimeter dust continuum observations. The well-studied starless core, L1544, appears to belong to the bar fragmentation type. We expect it to produce a highly elongated, opaque bar at the center in the future, which should break up into fragments of initial masses in the substellar regime.

Subject headings: binaries: formation — ISM: clouds — ISM: magnetic fields — MHD — stars: formation

1. INTRODUCTION

Most main-sequence stars are found in binary or low-order multiple-star systems (Duquennoy & Mayor 1991; Fischer & Marcy 1992). Recent observations of star-forming regions have revealed that the binary frequency of pre-main sequence stars is as high as or even higher than that of the main-sequence stars (Leinert et al. 1993; Ghez et al. 1997; Kohler et al. 2000; Mathieu et al. 2000). For example, in the well-studied nearby low-mass star forming Taurus-Auriga region, the binary frequency of pre-main sequence stars is a factor of two higher than that of the main-sequence stars. Other star-forming regions such as Ophiucus, Lupus, Chamaeleon, Scorpius-Centaurus, and

Corona Australis show a similar excess of binary fraction. Observations of binary stars in young star clusters such as Orion and Pleiades indicate that the binary frequency of the pre-main sequence stars is comparable to that of the main-sequence stars (Prosser et al. 1994; Padgett et al. 1997; Bouvier et al. 1997). These observations suggest that binary formation is the primary mode of star formation and that binaries should form prior to the pre-main sequence phase, most likely through fragmentation during the gravitational collapse of the parent dense molecular cloud cores (Mathieu 1994; Bodenheimer et al. 2000; White & Ghez 2000). Recent detections of binaries and multiple systems at the earliest observable phases of star

formation (e.g., Class 0 and Class I) support the fragmentation scenario (e.g., Wootten 1989; Fuller, Ladd, & Hodapp 1996; Looney et al. 1997, 2000; Terebey & Padgett 1997). How the fragmentation occurs is a long-standing, unresolved problem.

Many theoretical studies of star formation have concentrated on the formation of single stars (Shu, Adams, & Lizano 1987). In the standard picture of single star formation, a strongly magnetized dense molecular cloud core is taken as the initial state of star formation. The dense core gradually contracts as the magnetic support weakens in the high density part due to the ambipolar diffusion. When the magnetic field becomes too weak, it is overwhelmed by self-gravity, and the cloud begins a dynamic contraction to form a star. The process of magnetic leakage during the cloud contraction has been extensively investigated both analytically (e.g., Mestel & Spitzer 1956; Nakano & Tademaru 1972) and numerically (e.g., Nakano 1979; Black & Scott 1982; Lizano & Shu 1989; Ciolek & Mouschovias 1993; Basu & Mouschovias 1994; Li 2001). Specific models based on this scenario appear able to explain the observations of well-studied dense cores B1 and L1544 (Crutcher et al. 1994; Ciolek & Basu 2000; Li et al. 2002). However, these studies have assumed axisymmetry of the model cloud, and are unable to address the issue of fragmentation. On the other hand, numerical hydrodynamic calculations of cloud fragmentation have neglected the effects of magnetic fields (e.g., Tohline 2002), which are potentially important or even critical.

To quantify the role of magnetic fields on cloud fragmentation, we have made a start in investigating the non-axisymmetric evolution and fragmentation of initially magnetically subcritical clouds, taking into account the effect of magnetic diffusion. Our ultimate goal is to elucidate the fragmentation process in magnetically supported clouds, and extend the current standard scenario of low-mass star formation to binaries and multiple systems.

Magnetically subcritical clouds are stable to both dynamical collapse and fragmentation (e.g., Tomisaka, Ikeuchi, & Nakamura 1988). Obviously, it is difficult to form binary or multiple stars by direct fragmentation of such clouds. Three-dimensional magnetohydrodynamic (MHD) simulations of magnetic cloud collapse have shown that a frozen-in magnetic field stifles cloud fragmentation (Dorfi 1982; Benz 1984; Phillips 1986a,b). In lightly ionized molecular clouds, however, ambipolar diffusion can initiate dynamical contraction in magnetically supercritical cores by redistributing the magnetic flux in the cloud. The supercritical cores can be unstable to fragmentation if they have masses well above the Jeans limit (e.g., Mestel & Spitzer 1956; Galli et al. 2001).

Recently, Boss (2000, 2002) carried out three-dimensional collapse calculations of initially magnetically supported clouds, taking into account several properties of magnetic fields approximately. He concluded that the cloud fragmentation is enhanced by magnetic fields because the magnetic tension allows more time for the perturbations to grow off center nonlinearly, which presents the formation of a single, dominant object at the center. Li (2001) studied ambipolar diffusion-driven collapse of magnetized cloud cores with one-dimensional axisymmetric calculations but treating the magnetic forces and am-

bipolar diffusion more accurately. He also found a similar beneficial effect of magnetic tension. He classified the evolution of magnetically subcritical axisymmetric clouds into two types, depending mainly on the initial cloud mass and initial density distribution. When the initial cloud has a relatively low mass and/or a centrally-condensed density distribution, it collapses to form a single supercritical core (*core-forming cloud*). On the other hand, when the initial cloud is more massive (containing several Jeans masses or more) and has a relatively flat density distribution, it collapses to form a ring after the central region becomes magnetically supercritical (*ring-forming cloud*). One-dimensional axisymmetric evolution of the core-forming clouds has also been extensively investigated by Ciolek & Mouschovias (1993) and Basu & Mouschovias (1994). Li & Nakamura (2002) examined the ring-forming clouds and showed that they can fragment into multiple cores in the presence of non-axisymmetric density fluctuations during the isothermal collapse phase after the supercritical core formation. This type of ring fragmentation produces fragments of relatively large initial separations ($\sim 10^4$ AU). It may be responsible for the formation of small stellar groups such as those in the Serpens cloud core (Williams & Myers 2000) and aggregates of pre-stellar cores such as those in the ρ Oph B2 core (Motte, Andre, & Neri 1998) and around IRAS 03256+3055 in Perseus (Young et al. 2002). These studies illustrate the crucial role of magnetic diffusion in the fragmentation of magnetic clouds, with strong implications for binary formation.

In this paper, we focus on the non-axisymmetric evolution of the core-forming clouds, with an eye of the formation of binary stars. Initial results are presented in Nakamura & Li (2002), where we demonstrated that the core-forming clouds become unstable to a bar mode after the supercritical core formation [see also Nakamura & Hanawa (1997) for initially magnetically supercritical clouds]. Here, we extend the calculations to a larger parameter regime. First, we briefly describe our numerical method and model in §2. In §3, we examine the dependence of bar growth on the initial parameters such as magnetic strength, initial cloud mass, density profile, and rotation. We show that the core-forming clouds become unstable to a bar mode during the dynamic collapse phase over a wide range of initial model parameters. Subsequent fragmentation process is investigated in §4. Based on the numerical results, we classify the fragmentation process into three types, which agree with the empirical classification of young binary and multiple systems by Looney et al. (2000) based on high-resolution millimeter observations. This general agreement and other implications of our results on binary formation are discussed in §5.

2. FORMULATION OF THE PROBLEM

A detailed description of the model cloud and the problem formulation are presented in §2 of Li & Nakamura (2002). Here, we give a brief summary. We consider an initially axisymmetric, magnetically subcritical model cloud that is in a mechanical equilibrium, with a disk-like mass distribution due to settling along ordered magnetic field lines. In such a subcritical cloud, force balance along the field lines is achieved during the quasi-static phase of evolution and is well maintained even during the subse-

quent dynamic collapse (e.g., Fiedler & Mouschovias 1993; Nakamura, Hanawa, & Nakano 1995). Thus, we adopt the standard thin-disk approximation in which exact force balance along the vertical direction is assumed during the entire evolution (e.g., Ciolek & Mouschovias 1993; Basu & Mouschovias 1994; Shu & Li 1997; Nakamura & Hanawa 1997; Stehle & Spruit 2001; Li 2001). The magnetohydrodynamical equations are integrated in the vertical direction and the cloud evolution is followed in the $(x-y)$ disk plane of a Cartesian coordinate system (x, y, z) with a two-dimensional MHD code. The distribution of magnetic field is computed in three-dimensional space under the assumption that the magnetic field is current-free outside the disk.

We assume an isothermal equation of state below a dimensionless surface density Σ_{cr} , and denote the isothermal sound speed by c_s . Beyond Σ_{cr} , we change the equation of state from isothermal to adiabatic, with an index of $5/3$, to mimic the transition to optically thick regime of cloud evolution. In this paper, we set $\Sigma_{\text{cr}} = 1.9 \times 10^4 \Sigma_{0,\text{ref}}$, corresponding to the volume density $\rho_{\text{cr}} \sim 10^{12} \text{ cm}^{-3}$ (see eq. [1] below for the definition of $\Sigma_{0,\text{ref}}$).

The initial conditions for star formation are not well determined either observationally or theoretically. Following Basu & Mouschovias (1994) and Li (2001), we prescribe a slowly-rotating, axisymmetric reference state for our model cloud, with the distributions of mass, magnetic field, and velocity given by

$$\Sigma_{\text{ref}}(x, y) = \frac{\Sigma_{0,\text{ref}}}{[1 + (r/r_0)^n]^{4/n}}, \quad (1)$$

$$B_{z,\text{ref}}(x, y) = B_{z,\infty} = \text{const.}, \quad (2)$$

$$V_\phi(x, y) = \frac{4 \omega r}{r_0 + \sqrt{r_0^2 + r^2}} c_{ms}, \quad (3)$$

where $r = (x^2 + y^2)^{1/2}$ is the distance from the origin, $c_{ms} = c_s(1 + \Gamma_0^2)^{1/2}$ is essentially the magnetosonic speed, and the parameter ω measures the rotation rate. The exponent n controls the surface density profile and (indirectly) the amount of mass in the central plateau region where the distribution is more or less uniform. The background field strength $B_{z,\infty}$ is characterized by the dimensionless flux-to-mass ratio $\Gamma_0 = B_{z,\infty}/(2\pi G^{1/2} \Sigma_{0,\text{ref}})$. The reference clouds are not in an equilibrium state and are allowed to evolve into one with magnetic field frozen-in, before ambipolar diffusion is turned on at time $t = 0$. To save computational time, we obtain the equilibrium state using the one-dimensional axisymmetric MHD code of Li (2001), which gives results indistinguishable from those from the two-dimensional code assuming axisymmetry.

At $t = 0$, we impose on top of the equilibrium surface density $\Sigma_0(x, y)$ an $m = 2$ perturbation of relative amplitude A ,

$$\Sigma(x, y) = \Sigma_0(x, y) [1 + A \cos(2\phi)], \quad (4)$$

where ϕ is the azimuthal angle measured from the x -axis. The subsequent, ambipolar diffusion-driven evolution of the perturbed cloud is followed numerically with the two dimensional MHD code. As a boundary condition, we fixed ρ and B_z at the cloud outer radius, taken to be twice the characteristic radius r_0 .

The computations are carried out using non-dimensional quantities. The units we adopted are c_s for speed, $\Sigma_{0,\text{ref}}$

for surface density, $2\pi G \Sigma_{0,\text{ref}}$ for gravitational acceleration, and $B_{z,\infty}$ for magnetic field strength. The units for length and time are, respectively, $L_0 \equiv c_s^2/(2\pi G \Sigma_{0,\text{ref}})$ and $t_0 \equiv c_s/(2\pi G \Sigma_{0,\text{ref}})$. They have typical values of

$$L_0 = 8.43 \times 10^{-2} \text{ pc} \left(\frac{c_s}{0.33 \text{ km s}^{-1}} \right)^2 \left(\frac{\Sigma_{0,\text{ref}}}{10^{-2} \text{ g cm}^{-2}} \right)^{-1} \quad (5)$$

$$t_0 = 2.50 \times 10^5 \text{ yr} \left(\frac{c_s}{0.33 \text{ km s}^{-1}} \right) \left(\frac{\Sigma_{0,\text{ref}}}{10^{-2} \text{ g cm}^{-2}} \right)^{-1}, \quad (6)$$

where $c_s = 0.33 \text{ km s}^{-1}$ corresponds to an effective temperature of $T_{\text{eff}} = 30 \text{ K}$.

The initial state of our model cloud is completely specified by four parameters: the characteristic radius r_0 , exponent n in the reference surface density distribution, dimensionless flux-to-mass ratio Γ_0 , and rotation parameter ω . We adopt a relative small rotation parameter of $\omega \lesssim 0.2 - 0.3$, consistent with the slow rates of rotation observed in molecular cloud cores (Goodman et al. 1993). The slow rotation is thought to be due to magnetic braking by an ambient medium (Nakano & Tademaru 1972; Basu & Mouschovias 1994), which is not treated in our paper. We comment briefly on the potential effects of magnetic braking in § 5.3.

Besides the four parameters characterizing the initial cloud, a parameter A is needed to specify the fractional amplitude of the $m = 2$ bar mode perturbation applied after the reference cloud settles into the equilibrium configuration. We have carried out a systematic parameter survey and selected the models listed in Table 1 to illustrate the salient features of magnetic cloud evolution. The numerical results are described in the next two sections (§3 and §4).

3. BAR GROWTH IN MAGNETICALLY SUBCRITICAL CLOUDS

As mentioned earlier, Li (2001) classified the evolution of magnetically subcritical axisymmetric clouds into two types, depending mainly on the initial cloud mass and initial density distribution: (a) *core-forming cloud*, which collapses to form a single supercritical core and (b) *ring-forming cloud* in which a supercritical ring is formed after the central region becomes supercritical owing to ambipolar diffusion. The ring fragments into multiple supercritical cores in the presence of density fluctuations during the isothermal collapse phase (Li & Nakamura 2002). In this paper, we focus on the core-forming clouds and show that these clouds become unstable to bar formation after the supercritical core formation over a wide range of initial model parameters. The subsequent evolution and fragmentation of the bar are discussed in §4.

3.1. Non-Rotating Cloud

To begin with, we consider a non-rotating ($\omega = 0$) cloud with the reference state specified by the set of parameters $r_0 = 10\pi$, $n = 2$, and $\Gamma_0 = 1.5$. The cloud is therefore magnetically subcritical, with the field strength 50% above the critical value at the center. The cloud so specified produces a dense supercritical core in the absence of any non-axisymmetric perturbations. The reference cloud is allowed to evolve into an equilibrium configuration, with the

magnetic field frozen-in. After the equilibrium is reached, we reset the time to $t = 0$, turn on ambipolar diffusion, and add an $m = 2$ perturbation to the surface density distribution, with a fractional amplitude of $A = 0.05$. The evolution of such a non-axisymmetrically perturbed cloud is followed numerically to progressively higher densities and smaller scales. The results are shown in Fig. 1 and described as follows.

The evolution of the model is qualitatively similar to that of the model shown in Fig. 1 of Nakamura & Li (2002), where a different reference density distribution (less centrally-condensed than the model shown in this subsection) is adopted. The evolution is followed to a higher density here. As is usual with ambipolar diffusion-driven evolution, the cloud spends most of its time in the subcritical phase when the dimensionless minimum flux-to-mass ratio (at the density peak) is greater than unity, $\Gamma_c > 1$ (see panels [a] and [b] of Fig. 1). During this period, gas motions are very subsonic and the central part of the cloud oscillates with a small amplitude. The oscillation indicates that the cloud is stable to the $m = 2$ perturbation during the subcritical phase, in agreement with linear analysis by Nakano (1988) and others. Indeed, we have verified numerically that for a frozen-in field the subcritical cloud remains stable to this and other higher (e.g., $m = 3, 4, \dots$) modes. (We followed the evolution of the frozen-in model for several periods of oscillation and confirmed that the cloud oscillates with almost the same amplitude as the initial.) Once the minimum flux-to-mass ratio has dropped below the critical value, the contraction becomes dynamic and the infall speed eventually exceeds the sound speed at the center (see panels [c] and [d]). By the time shown in panel (c), the $m = 2$ mode has grown significantly, resulting in a bar-like core at the center with an aspect ratio of roughly 2. The bar growth remains relatively modest (panel [d]) until the very end of the runaway collapse, when the growth rate increases dramatically (panel [e]). Beyond a dimensionless critical surface density of 1.9×10^4 , corresponding to a volume density of $n_H \sim 10^{12} \text{ cm}^{-3}$, we change the equation of state from isothermal to adiabatic, with an index of $5/3$, to mimic the transition to optically thick regime of cloud evolution. When the maximum surface density reaches $\sim 10^5$, the contraction along the minor axis of the bar decelerates significantly and an accretion shock is formed at the surface of the bar. This shock-bound bar is analogous to the “first core” of spherical calculations, and will be referred to as the “first bar” below. Immediately after the shock formation, the aspect ratio of the first bar continues to increase. It reaches a maximum of about 10 by the time shown in panel (e). Thereafter, the infall along the major axis becomes significant, forming a round core at the center. The aspect ratio of the central round core approaches unity as the collapse proceeds. Since the round core resembles the first core of the spherical calculations, we call it the “truly first core”. As will be shown in §4, this round core evolves into a rapidly-rotating disk in the presence of an initial, slow cloud rotation.

To quantify the geometrical change of the supercritical core, we plot in Figure 2 the aspect ratio of the darkest region in Figure 1 (with $\Sigma > 10^{-1/2}\Sigma_{\text{max}}$) as a function of the maximum surface density, Σ_{max} , together with the

flux-to-mass-ratio Γ at the center. The aspect ratio is defined as $R = a_y/a_x$ where a_x and a_y are, respectively, the effective scale heights along the x and y axes, and evaluated as

$$a_x = \left(M^{-1} \int_{\Sigma \geq 10^{-1/2}\Sigma_{\text{max}}} \Sigma x^2 dx dy \right)^{1/2}, \quad (7)$$

and

$$a_y = \left(M^{-1} \int_{\Sigma \geq 10^{-1/2}\Sigma_{\text{max}}} \Sigma y^2 dx dy \right)^{1/2}, \quad (8)$$

where M is the total mass in the region with $\Sigma \geq 10^{-1/2}\Sigma_{\text{max}}$. During the subcritical phase, the aspect ratio of the bar does not grow in time; it oscillates around unity, signifying that the subcritical cloud is stable to the $m = 2$ mode. As the central region becomes more and more supercritical, the bar mode begins to grow significantly. During this supercritical period, the aspect ratio of the bar stays more or less frozen at $R \sim 1.5$ before the central density reaches $\Sigma \sim 10^3$. This freezing of aspect ratio is related to the dynamical state of the disk. As shown in §3.4, the mass of the central flat region is merely ~ 1.5 times the effective Jeans mass (as measured by the central surface density, including the magnetic contribution). Such a relatively low-mass disk is only marginally unstable to the non-axisymmetric perturbation. In other words, the time scale of bar growth is comparable to that of dynamic contraction. The flux-to-mass ratio does not change much either during this period, as a result of the rapid collapse which prevents the magnetic flux from leaking out significantly. The bar growth speeds up toward the very end of the supercritical collapse when the mass of the central flat region exceeds about twice the effective Jeans mass. It continues after the first bar formation. When the central surface density reaches 10^5 , the infall motion along the major axis of the bar becomes significant and the aspect ratio begins to drop steeply to unity, forming the truly first core.

To study the structure of the bar, we show in Figure 3 the distributions of the surface density, magnetic field, and infall velocity along the axes as a function of the distance from the density maximum, at seven different times. The solid and dashed curves indicate the distributions of the physical quantities along the major (y) and minor (x) axes, respectively. During the early phase of supercritical collapse when the aspect ratio of the bar is frozen at $R \sim 1.5$, the surface density distributions along both axes qualitatively resemble the self-similar distribution of the axisymmetric collapse; they are flat near the density maximum and can be approximated by a power-law of $\Sigma \propto d^{-1}$ at the magnetically supercritical envelope, where d is the distance from the density peak. The $\Sigma \propto d^{-1}$ distribution corresponds to a volume density distribution of $\rho \propto d^{-2}$ because of the force balance in the vertical direction (which yields $\rho \propto \Sigma^2$). While the central density increases rapidly, the surface density distributions change little in the envelope. The central flat region shrinks in size in accordance with the increase in the central density. The distributions of the vertical field B_z are qualitatively similar to those of Σ in the magnetically supercritical region and almost proportional to the local surface density ($B_z \propto \Sigma$). The x - and y -components of the magnetic field (in the disk plane) increase approximately linearly with distance d in

the central flat region, peaking near the edge of the flat region, before falling off as $B_x \propto d^{-1}$ and $B_y \propto d^{-1}$. In the magnetically supercritical envelope, B_x and B_y are comparable to B_z , indicating that the field lines near the disk plane incline with an angle of ~ 45 degree with respect to the disk plane. The angle approaches ~ 90 degree in the outer, magnetically subcritical envelope. The infall speeds are proportional to the distance d near the center, becoming more or less flat in the supercritical part of the envelope, before falling to subsonic values in the outer subcritical envelope. At $\Sigma_{\max} = 10^4$, the infall speeds in the supercritical envelope reach $\sim 2c_s$.

As the collapse proceeds and the bar aspect ratio becomes large, the distributions of physical quantities gradually deviate from the self-similar distributions. For example, the surface density and vertical magnetic field (B_z) profiles along the major axis become steeper as the bar elongates rapidly. When the central surface density reaches $\sim 2 \times 10^4$, a shock is formed at $x \sim 10^{-4}r_0$. Thereafter, the infall speed rises in the envelope of the bar. The infall speed along the minor axis follows $v_x \propto d^{-1/2}$ just outside the first bar, indicating a free-fall collapse towards the bar.

Interestingly, after the bar becomes opaque to dust emission, a local density peak is formed at each end of the first bar. This density peak formation is due to the “edge” effect, which was first calculated by Larson (1972) and then extensively investigated by Bastien (1983) and Bonnell & Bastien (1991). In this model, the density peaks do not grow nonlinearly; they tend to disappear in the subsequent collapse because the central truly first core grows more rapidly in mass owing to the supersonic infall along the major axis, which dominates the gravitational potential in the high density region. In §4, we show that for more massive clouds in which the aspect ratios of the supercritical cores are larger, the density peaks *can* grow in time because the infall speeds along the major axis remain subsonic.

The model discussed in this subsection serves as a standard against which other models will be compared.

3.2. Dependence of Model Parameters: Γ_0 , r_0 , and n

The properties of the bar growth depend on the initial model parameters. Here, we investigate the effects of the initial flux-to-mass ratio Γ_0 , the characteristic radius r_0 , and the density profile parameter n for non-rotating clouds. The effect of rotation is examined in separate subsections §3.3 and §4.1. Exact values of Γ_0 are difficult to determine observationally; they probably lie within a factor of two of unity (Crutcher 1999), after correcting for likely projection effects (Shu et al. 1999). Thus, we investigated the dependence on Γ_0 in the range of $1 \lesssim \Gamma_0 \lesssim 3$. The characteristic radius r_0 is to be compared with 2π , the (dimensionless) critical wavelength for the (thermal) Jeans instability in a disk of uniform mass distribution (Larson 1985). The parameter n controls the profile of the cloud surface density distribution; those with smaller values of n are more centrally peaked.

To examine the effect of the initial flux-to-mass ratio Γ_0 , we first hold the cloud radius and profile parameter

fixed at the standard values $r_0 = 10\pi$ and $n = 2$, and reduce the flux-to-mass ratio Γ_0 . Representative results are shown in panel (a) of Fig. 4, at a time when the maximum surface density $\Sigma_{\max} = 10^4$. Panel (a) is the snapshot of a cloud with $\Gamma_0 = 1.25$ (a weaker initial magnetic field), perturbed by an $m = 2$ mode of the standard fractional amplitude $A = 0.05$. Comparison with panel (d) of Fig. 1 where the standard case at the same Σ_{\max} is plotted shows that a weaker magnetic field promotes the bar growth. This slower bar growth in the stronger field case is quantitatively shown in panel (a) of Figure 2 (compare the solid curve with the dotted-dashed curve). The reason for this behavior appears to be that, for the cloud with a stronger initial magnetic field, the magnetic support remains more important even in the supercritical phase. In other words, the averaged flux-to-mass ratio in the darkest region ($\Sigma \geq 10^{-1/2}\Sigma_{\max}$) is larger for the stronger field model. The stronger field tends to retard the deformation of the supercritical core. We have confirmed this negative effect of the magnetic field on bar growth by following the evolution of the clouds with $\Gamma_0 = 2$ and 3.¹

We next consider the effect of the characteristic radius r_0 which controls the total cloud mass. Increasing the radius r_0 is expected to have a positive effect on bar growth. This is indeed the case, as illustrated in panel (b) of Fig. 4, where the snapshot of a cloud with $r_0 = 15\pi$, 1.5 times the standard value, is shown at $\Sigma_{\max} = 10^4$. The aspect ratio of the bar reaches ~ 7 at the time when the surface density reaches 10^4 .

The profile parameter n has an effect similar to the parameter r_0 . For instance, a reduction in n would decrease the number of Jeans masses contained in the central plateau region. We showed in a previous paper (Li & Nakamura 2002) that for the ring-forming case, the clouds with more peaked density profiles are less prone to fragmentation. This negative effect of the centrally condensed density distribution is also observed for non-magnetized clouds (Boss 1993). We find the same trend for the core-forming clouds as well. The aspect ratio of the bar increases more rapidly for larger n . This is illustrated in panel (c) of Fig. 4, where $n = 4$, twice the standard value, is chosen. The bar is more elongated than the standard case, even though the characteristic radius $r_0 = 5\pi$ is only half of the standard value.

3.3. Slowly-Rotating Cloud

To gauge the effect of slow rotation, we repeat the evolution of a cloud with all parameters identical to those of the standard model in §3.1 except the rotation parameter ω , which is now set to 0.1 instead of zero. Snapshots of the surface density distribution and velocity field at three selected times are shown in Fig. 5. The general trend of the cloud evolution is similar to that in the non-rotating case; in the subcritical phase, the cloud is stable to non-axisymmetric perturbations and the $m = 2$ mode begins to grow in time only after the central region becomes magnetically supercritical. Comparison between Fig. 1d and Fig. 5b indicates a beneficial effect of the slow rotation on the bar growth. More quantitatively, the aspect ratio of

¹ We note that the magnetic field has an opposite, beneficial effect on the fragmentation of ring-forming clouds. More strongly magnetized clouds contract more slowly, allowing more time for non-axisymmetric perturbations to grow off-center. As a result, multiple fragmentation is achieved more readily, at a lower surface density. See Li & Nakamura (2002) for details.

the bar is always larger for the rotating cloud at the time when the maximum density reaches the same value, before the bar becomes opaque to dust emission. This effect derives from the fact that rotation retards the radial infall, which allows more time for perturbations to grow.

In §4.1 below, we will show that the slow-down effect due to rotation plays a dramatic role in the cloud fragmentation for more rapidly-rotating, less centrally-condensed clouds, which can fragment into two cores during the isothermal collapse phase soon after the supercritical core formation.

3.4. Dynamical State of Supercritical Cores: Axisymmetric Collapse

The bar growth is closely related to the dynamical state of the supercritical core. In this subsection, to clarify the physics of the bar growth, we follow the evolution of unperturbed axisymmetric clouds with the one-dimensional code and measure the dynamical forces in the supercritical cores. For simplicity, we do not change the equation of state for the one-dimensional calculations even when the surface density exceeds the critical value of 1.9×10^4 . Previous axisymmetric calculations of ambipolar diffusion-driven cloud evolution have shown that the collapse of supercritical cores proceeds self-similarly: the distributions of the surface density and magnetic field are almost constant in the central flat region and decrease with radius as $\Sigma \propto r^{-1}$ and $B_z \propto r^{-1}$ (Ciolek & Mouschovias 1993; Basu & Mouschovias 1994). In the high density region of the supercritical core, the decrease of the flux-to-mass ratio levels off (at $\Gamma \sim 0.4$) due to the rapid dynamic collapse which prevents significant magnetic flux leakage. This is shown in panels (a) and (c) of Figure 6, where the flux-to-mass ratio normalized by the critical value is depicted as a function of radius for two representative models. Shu & Li (1997) and Li & Shu (1997) called such a cloud with a constant flux-to-mass ratio “isopedic”. In the isopedic cloud, the gravity ($F_{\text{grav}} = \Sigma g_r$) and gas pressure ($F_{\text{gas}} = c_s^2 d\Sigma/dr$) are proportional to the magnetic tension ($F_{\text{ten}} = B_r B_z / 2\pi$) and pressure ($F_B = Hd(B_z^2/4\pi)/dr$), respectively (Shu & Li 1997; Li & Shu 1997; Nakamura & Hanawa 1997), where H is the half thickness of the disk (see eq. [5] of Li & Nakamura (2002) for the definition of H). In fact, the supercritical cores have such a characteristic.

Figure 6 shows the evolution of the ratio of the effective gravity to the effective pressure at six different times for two models. Here, the effective pressure and gravity are defined as $F_{\text{gas}} + F_B$ and $F_{\text{grav}} + F_{\text{ten}}$, respectively. At the initial state ($t = 0$), this ratio is equal to unity, indicating a force balance in the initial cloud. As the collapse proceeds, this ratio increases due to ambipolar diffusion, which reduces the magnetic support in the central high density region. When the central surface density is in the range of $10^3 - 10^4$, the effective gravity is larger than the effective pressure, but only by a factor of about 1.5 – 2. This corresponds to a mass of the central flat region only about 1.5 – 2 times the effective Jeans mass. Such a relatively low-mass core is only marginally unstable to non-axisymmetric perturbations, which is probably the reason why the aspect ratio of the bar remains almost frozen at a modest value of 1.5 – 2 in the presence of an $m = 2$ perturbation.

When the force ratio exceeds ~ 2 , the bar growth is accelerated remarkably by the Lin-Mestel-Shu type gravitational instability (Lin, Mestel, & Shu 1965), as seen in Fig. 2. For both clouds, the force ratios approach a higher value of 3 – 4 as the collapse proceeds, although a convergence hasn’t been reached by the time the central surface density reaches the critical value of 1.9×10^4 . (The convergence toward a self-similar solution is slower for more centrally-condensed clouds.) This behavior suggests that the isothermal evolution tends toward a self-similar solution.

A self-similar solution reproducing the pre-protostellar collapse of an isopedic magnetic disk is derived approximately by Nakamura & Hanawa (1997), who considered a frozen-in magnetic field [see also Saigo & Hanawa (1998) for the nonmagnetized case]. Basu (1997) constructed a self-similar collapse model including the effect of ambipolar diffusion [see Li (1998) for the self-similar collapse after the protostellar core formation]. The behavior of his solution is in good agreement with that of Nakamura & Hanawa (1997) in the late, self-similar phase of dynamic collapse, when the effective gravity is about 3 – 4 times the effective pressure force and the asymptotic velocity is about twice the effective sound speed. Nakamura & Hanawa (1997) investigated the dynamical stability of the self-similar solution to non-axisymmetric perturbations and found that the self-similar solution is unstable to the $m = 2$ mode and stable to the higher modes. This characteristic is consistent with the numerical results presented in the previous subsections. Thus, we conclude that the tendency for the supercritical collapse to approach the gravity-dominated self-similar solution is responsible for the bar formation during the dynamic collapse.

4. FRAGMENTATION OF SUPERCRITICAL CORES

In §3, we demonstrated that initially magnetically subcritical clouds tend to be unstable to an $m = 2$ mode, forming bar-like cores. In this section, we investigate the subsequent evolution of the bar mode and show that the elongated supercritical cores can break up into discrete fragments. We classify the fragmentation process into three types, depending on the initial model parameters: (1) *separate core formation*, in which the $m = 2$ mode breaks up into two separate cores in the isothermal collapse phase, (2) *bar fragmentation*, in which the first bar breaks up into multiple fragments that move mainly along the major axis of the bar, with frequent merging among the fragments, and (3) *disk fragmentation*, in which the central region evolves into a rapidly-rotating disk where another bar mode is excited, fragmenting into blobs. In the following, we select three models to illustrate the salient features of these cases.

4.1. Separate Core Formation: Effect of Faster Rotation

In §3.3, we showed that rotation slows down the dynamic collapse, allowing more time for perturbations to grow. Here, we demonstrate that a relatively fast rotation can affect the outcome of cloud evolution dramatically, particularly for $n \gtrsim 4$ clouds whose initial parameter range is intermediate between those for core-forming and ring-forming clouds in the axisymmetric calculations (Li 2001). Panels (b) and (c) of Fig. 7 show the snapshots of

the surface density distribution and velocity field at two selected times for the model with $n = 4$, $\omega = 0.2$, $r_0 = 5\pi$, and $\Gamma_0 = 1.5$. This cloud is categorized as a core-forming cloud from the axisymmetric one-dimensional calculation. A cloud larger in radius by only a few tens of percent would collapse to form a ring instead of a single core. For comparison, the snapshot of a more slowly rotating cloud with $\omega = 0.1$ is shown in panel (a) at the time when $\Sigma_{\max} = 10^2$. The model with $\omega = 0.1$ shows the evolution qualitatively similar to the model in §3.3, i.e., after the supercritical core formation, a bar mode grows in time without fragmentation. On the other hand, when the rotation rate is doubled ($\omega = 0.2$), the bar grows more rapidly even at the early time shown in panel (b), when the maximum surface density reaches 10. By this time, the entire bar (the darkest part in panel [b]) becomes magnetically supercritical. By the time shown in panel (c) ($\Sigma_{\max} = 10^2$), the $m = 2$ mode breaks up into two separate cores, each of which continues to collapse dynamically. (We checked that this model is stable to higher m modes.) The subsequent evolution of each core is qualitatively similar to that of the models shown in the previous section, i.e., the aspect ratio of each core is more or less frozen at ~ 2 during the early phase of supercritical collapse, and increases rapidly at the very end of the supercritical collapse.

For the separate core formation case, the magnetic field has a positive effect on the fragmentation. We calculated the models of a weaker and a stronger magnetic field for the same set of parameters $n = 4$, $r_0 = 5\pi$, $\omega = 0.2$, and $A = 0.05$, and found that the cloud with a weaker magnetic field does not break up into two cores (it collapses into a single bar instead), whereas the cloud with a stronger magnetic field fragments into two cores at a lower density and with a wider separation. More centrally-condensed clouds with $n = 2$ and $r_0 \lesssim 20\pi$ do not fragment into two cores even in the presence of a rapid rotation ($\omega \sim 0.3$). These dependences on Γ_0 and n are the same as those of the multiple fragmentation case investigated by Li & Nakamura (2002). In this sense, the separate core case is similar to the multiple fragmentation case, although the bar fragmentation into two cores appears to depend more strongly on the rotation rate.

At the time shown in panel (c), the separation of two cores is about a tenth of the initial cloud radius, which corresponds to 5×10^4 AU with the fiducial choice of $\Sigma_0 = 0.01$ g cm $^{-2}$ and $T_{\text{eff}} = 30$ K. This separate core formation case may thus be responsible for the formation of wide binaries with separations of the order of 10^4 AU, although substantial orbital evolution is likely after the initial fragmentation, since the cores are not kept apart by rotation.

To summarize, when the initial rotation is relatively fast and the density distribution in the central region is relatively flat, the $m = 2$ mode can break up into two separate cores in the isothermal collapse phase after the central region becomes supercritical (e.g., for $n = 4$, $\omega \sim 0.2$, $\Gamma_0 \sim 1.5$, and $r_0 \gtrsim 5\pi$). We note that this separate core formation differs from that found previously for non-magnetic clouds, which requires a rapid rotation or highly unstable initial condition (e.g., Tsuribe & Inutsuka 1999). In our case, the cloud is initially stable to gravitational collapse, and the fragmentation is induced by ambipolar diffusion. Indeed, we find that clouds with relatively weak

magnetic fields do not fragment into separate cores during the isothermal collapse phase.

4.2. Bar Fragmentation and Merging of Fragments

According to linear perturbation theory, long filamentary clouds tend to break up gravitationally into fragments if their lengths exceed several times the diameter. This is indeed the case for the first bars formed in relatively massive, centrally-condensed clouds (with a relatively large r_0 and $n \lesssim 4$, e.g., for $n = 2$, $\Gamma_0 \sim 1.5$, $\omega \sim 0.2$, and $r_0 \gtrsim 15\pi$), as illustrated in Fig. 8, where the snapshots of a cloud with $n = 2$, $\Gamma_0 = 1.5$, $r_0 = 15\pi$, and $\omega = 0.2$ are shown at three different times. In this model, fragmentation starts when the bar becomes opaque to dust emission, which retards the radial contraction (at $\Sigma_c \gtrsim 10^5$). At first, the bar produces two dense fragments near the center at $\Sigma \sim 10^5$, and then the fragmentation apparently propagates towards the ends of the bar. This apparent propagation of the fragmentation is due to the fact that the growth rate of the gravitational fragmentation is larger for the higher density region closer to the center. By the time shown in panel (a), there is a fragment formed at each of the two ends of the bar. This density peak formation at the end was first noticed by Larson (1972) and subsequently investigated extensively by Bastien (1983) and Bonnell & Bastien (1991). It is caused by a local minimum in the gravitational potential. The masses of the fragments formed by bar fragmentation are on the order of $10^{-2} M_\odot$. These masses agree with those expected from the linear theory of fragmentation of cylindrical clouds (e.g., Larson 1985; Nakamura, Hanawa, & Nakano 1993). By the time shown in panel (b), the two pairs of fragments near the center have merged to produce one, more massive, pair. This process of successive bar fragmentation and subsequent merging is repeated, as shown in panel (c), where the two most massive fragments are about to merge at the center. We will discuss further the evolution of this multiple fragment system in §5.

We note that bar fragmentation was also observed in the numerical simulations of non-magnetic cloud collapse (e.g., Boss 1993; Bate & Burkert 1997). The non-magnetic bars are typically much shorter than the one presented in this subsection. To form such a long bar in the non-magnetic case, the initial cloud must contain many thermal Jeans masses and thus be highly unstable. In our case, the initial cloud is stabilized by a strong magnetic field, whose support weakens with time as a result of ambipolar diffusion. Nakamura & Hanawa (1997) studied bar formation in clouds with frozen-in magnetic fields. They found bars that are prone to gravitational breakup according to the linear theory of fragmentation. These bars are however shorter than the one discussed here. They are expected to produce a smaller number of fragments.

4.3. Disk Formation and Fragmentation

When the initial clouds are centrally condensed and/or less massive (e.g., for $n = 2$, $\omega \sim 0.1$, $\Gamma_0 \sim 1.5$, and $r_0 \lesssim 15\pi$), the length of the bar does not exceed the critical wavelength for gravitational fragmentation by the time of first bar formation. It would be difficult for such a short bar to break up into blobs gravitationally. In this case, a rapidly-rotating disk is formed in the presence of slow ro-

tation. Here, we show an example of the rotating disk formation. Figure 9 shows the snapshots at six different times of a model with $n = 2$, $\Gamma_0 = 1.5$, $r_0 = 5\pi$, and $\omega = 0.1$, which is identical to the slowly rotating model discussed in §3.3, except for a smaller characteristic radius r_0 (5π instead of 10π). For comparison, the linear density contours of the central disk is depicted in Fig. 10 at three selected times. In this model, the bar mode does not grow much by the end of isothermal collapse because of the relatively small cloud radius r_0^2 . Because the length of the bar is smaller than the critical wavelength for gravitational fragmentation, it does not fragment. Instead, a round dense region, which we called the “truly first core”, is formed at the center due to a supersonic infall motion along the bar.

Initially, the truly first core is supported primarily by the thermal pressure. As ambient gas with a larger angular momentum accretes onto it, the rotational support becomes dominant. As a result, the central core evolves into a rapidly-rotating, opaque disk, which we will sometimes refer to as the “first disk”. The interaction between the disk and the large-scale bar mode outside the disk excites another bar-mode growing inside the disk. We believe that the secondary bar growth is due to rotational instability because the ratio of the rotational energy and the gravitational energy of the first disk reaches the critical value of $\beta_{\text{cr}} \sim 0.3$ (e.g., Durisen et al. 1986; Bate 1998; Tohline 2002). By the time shown in panel (c) of Fig. 10, the bar breaks up into two blobs, which appear to be self-gravitating. We stopped our calculation at this epoch of fragmentation because the volume densities of the blobs reach the critical density beyond which H_2 dissociation starts and the equation of state of the gas is expected to change again.

The fate of the two blobs formed in the disk is uncertain. They may merge together during the subsequent evolution. Since the rotation period of the disk is faster than that of the large-scale bar outside the disk, the interaction between the two bar modes generates several blobs in the disk, some of which appear to be self-gravitating. These blobs are expected to interact gravitationally and whether any of them can survive the interaction remains to be determined. This type of fragmentation and merging in a rotating disk was also observed in the numerical simulations of non-magnetic cloud collapse (e.g., Bonnell 1994; Whitworth et al. 1995; Burkert et al. 1997; Matsumoto & Hanawa 2002).

5. DISCUSSION

5.1. Fragmentation of Magnetic Clouds

In the previous sections, we have shown that core-forming clouds tend to become unstable to the bar mode after the supercritical core formation. The numerical results presented in this paper and in Li & Nakamura (2002) indicate that fragmentation of magnetic clouds happens readily over a wide range of initial cloud parameters. On the surface, this result appears to contradict earlier numerical studies of magnetic cloud fragmentation, which

suggest that strong magnetic fields tend to stifle fragmentation of dynamically collapsing clouds (Dorfi 1982; Benz 1984; Phillips 1986a,b). For example, Phillips (1986a) performed three-dimensional MHD simulations on initially magnetically supercritical clouds and found that none of his clouds show any evidence for fragmentation even in the presence of a large density perturbation with a fractional amplitude of 50%. We emphasize that there are two important differences between our model and the previous ones. First, previous studies considered a frozen-in field, whereas in our study ambipolar diffusion is a crucial ingredient. Our initial cloud, which is supported by a strong magnetic field, is stable to gravitational fragmentation as well as dynamic collapse. The weakening of the magnetic support driven by ambipolar diffusion is what initiates the dynamic collapse and fragmentation. Second, the contribution of the magnetic tension to the cloud support is much weaker in the earlier studies; indeed, most of them took a uniform magnetic field as the initial state (which of course has no magnetic tension). The beneficial effect of magnetic tension on cloud fragmentation was discussed by Boss (2000, 2002), who showed that a strong magnetic tension can slow down cloud contraction appreciably, which tends to enhance cloud fragmentation.

Recently, Tohline (2002) reviewed the theoretical studies on binary star formation, concentrating on the non-magnetic case. He found broad agreement among numerical simulations by various groups that non-magnetic clouds are susceptible to prompt fragmentation if they collapse from an initial configuration that is relatively uniform in density and contains more than a few Jeans masses of material. If supported only by thermal pressure, such a configuration is highly unstable. The question is then (Tohline 2002): how is nature able to produce such an unstable configuration in the first place? We believe that the key to resolve this apparent difficulty is the presence of a strong magnetic field, which stabilizes the entire cloud even when the cloud mass is well above one thermal Jeans mass³ (e.g., Lizano & Shu 1989). Specific models of core formation in magnetically subcritical clouds appear able to explain the mass distribution and extended subsonic infall motions inferred in several starless cores (e.g., Lee, Myers & Taffala 2001; Ciolek & Basu 2000; Indebetouw & Zweibel 2000) and are consistent with pattern of chemical differentiation observed in L1544 (Li et al. 2002), provided that the initial flux-to-mass ratio lies within a factor of two or so of the critical value, as adopted in this paper.

5.2. Elongation of Dense Cloud Cores

Dense cores of molecular clouds are observed to have significant elongation, with a typical aspect ratio of 2 in the plane of sky (Myers et al. 1991). Their true three-dimensional shapes are probably triaxial, as inferred statistically by Jones, Basu & Dubinski (2001) and Goodwin, Ward-Thompson, & Whitworth (2002). We have previously noted that the triaxial core shape can naturally result from nonlinear growth of the bar mode in the direction perpendicular to the field lines, coupled with the flattening

² We estimate that the central plateau region of this cloud has a size roughly 2 – 3 times the effective Jeans length, judging from the fact that, for $n = 2$, reference clouds with $r_0 \lesssim 2\pi$ expand rather than contract.

³ The cloud can also be supported by turbulence, although the details of cloud evolution driven by turbulence decay remain to be worked out (Myers 1999).

of the mass distribution along the field lines (Nakamura & Li 2002). The models presented in §3 strengthen this conclusion. We find that the aspect ratio of the bar is more or less independent of the initial model parameters. It stays at about $1.5 - 2$ during the period when Γ decreases from ~ 1 to ~ 0.5 , after the core has become supercritical (which makes bar growth possible) but before the ratio of effective gravity to effective pressure force exceeds ~ 2 (when the bar elongation is greatly amplified through the Lin-Mestel-Shu instability). This initial period of supercritical phase is also the phase most likely observed as a starless core, when the core is dense enough to be identified as a core using high density tracers (such as NH_3 or CS), but before rapid collapse sets in which quickly produces a stellar object at the center, ending the starless phase.

In this supercritical collapse phase, the decrease of the central flux-to-mass ratio saturates at about half the critical value, almost independent of the initial parameters (see panel [b] of Fig. 2). This saturation of flux-to-mass ratio is also observed in axisymmetric models (Basu & Mouschovias 1995). It means that the supercritical cores remain significantly magnetized, and magnetic fields may not be completely ignored even during the dynamic collapse phase of star formation.

5.3. Three Types of Binary and Multiple Star Formation

Observations of nearby star forming regions have established that binary fraction among pre-main sequence stars is at least as high as among the main-sequence stars. In some nearby low-mass star forming regions like Taurus-Auriga, the binary frequency is even higher than that of main-sequence stars. In such low-mass star forming regions, stellar densities ($n_* \sim 10 \text{ pc}^{-3}$) are much too low to allow the formation of binaries by capture or their destruction by gravitational encounters within their ages of $\sim 1 \text{ Myr}$. This indicates that the observed high binary frequencies more or less reflect the pristine population of proto-binaries at the epoch of formation, suggesting that binary and small multiple stars are formed prior to pre-main sequence phase by gravitational fragmentation of parent dense molecular cloud cores. In fact, recent high resolution millimeter observations of dust continuum have revealed evidence of gravitational fragmentation of proto-stellar cores in the earliest, Class 0 and I phases. Such observations were summarized in Looney et al. (2000), who classified young multiple star systems into three types: (1) separate envelope (separation $\geq 6000 \text{ AU}$), (2) common envelope (separation $150 - 3000 \text{ AU}$), and (3) common disk systems (separation $\leq 100 \text{ AU}$). Separate envelope systems exhibit clearly distinct centers of gravitationally bound cores with separations greater than 6000 AU and the components are surrounded by low density material (e.g., NGC1333 IRS2, SVS13). Common envelope systems have one primary core of gravitational concentration which apparently breaks up into multiple fragments with separations of $100 - 3000 \text{ AU}$ (e.g., IRAS 16293-2422). Common disk systems have circumbinary disk-like envelopes surrounding young stellar objects with separations smaller than 100 AU (e.g., L1551 IRS5).

We have also uncovered three distinct types of fragmentation of magnetic clouds in our numerical experiments. They correspond roughly with the above empirical classi-

fication of young binary and multiple star systems. Based upon the results presented in §4, we classify theoretically the process of fragmentation into three types, depending on the initial model parameters: (1) *separate core formation*, in which the cloud breaks up into two separate cores during the isothermal collapse phase, (2) *bar fragmentation*, in which the aspect ratio of the bar becomes large enough to break up into multiple fragments along the major axis and the fragmentation takes place after the bar has become opaque to dust emission, and (3) *disk fragmentation*, in which the central region, after becoming opaque to dust emission, evolves into a rapidly rotating disk, which fragments into multiple blobs. These cases are discussed in turn.

When the initial cloud has a relatively flat central part and is rotating relatively rapidly (e.g., $\omega \sim 0.2$ for $n \sim 4$), it fragments into two separate cores during the isothermal collapse phase in the presence of an $m = 2$ perturbation after the central region becomes magnetically supercritical (*separate core formation*). Morphologically, this case resembles the separate envelope systems discussed in Looney et al. (2000). The early phase of fragmentation also looks like the double-core in the extinction map of Fes 1-457 (Alves et al. 2002) (see Laundardt [2001] for another example of double-core, in Bok globule CB 230). When first produced, the dense cores have insufficient orbital rotation to prevent them from spiraling towards each other. We expect their separation to shrink appreciably with time, producing perhaps a highly eccentric system. Whether they will eventually merge together is unclear at the present. We suspect that the cores will survive to become individual star/stellar system, since the density is much higher inside the cores than outside by the end of our calculations. This means that it takes the cores much less time to collapse onto themselves to form stars than to merge together. Moreover, there exists a strong magnetic field outside the cores which can prevent direct core collision. In our separate core formation case, the density of the central inter-core region decreases with time as matter falls towards the cores, whereas the field strength increases due to magnetic flux diffusion out of the cores into the inter-core region. Indeed, the central inter-core region may become magnetically subcritical again at the later stages of evolution. This region serves as a “magnetic cushion” to direct core collision. We propose that the separate core formation is a mechanism for producing wide binaries with separations of $\sim 10^4 \text{ AU}$. Each core will have a second chance at fragmentation at higher densities, when a first bar or rotating disk is formed. The secondary fragmentation within each core could lead to the formation of a small (hierarchical) multiple star system. As mentioned earlier, separate core formation in the presence of an $m = 2$ perturbation has much in common with the multiple fragmentation induced by higher order perturbations that we studied previously in Li & Nakamura (2002). Multiple core formation is an related channel for wide binary and multiple star formation.

When the initial cloud contains a mass well above the thermal Jeans mass and has a moderately centrally condensed density distribution (e.g., $r_0 \gtrsim 15\pi$ for $n \sim 2$ and $\omega \sim 0.1 - 0.2$), a long bar is formed, which can break up into several (pairs of) fragments after the bar becomes

opaque to the dust emission (*bar fragmentation*). The multiple fragments grow in mass due to both merging and accretion. This bar fragmentation case would correspond to the common envelope systems of Looney et al. (2000), since the whole bar is embedded within a common core out of which the bar is formed. The bar fragmentation occurs at a density of $\sim 10^{12} \text{ cm}^{-3}$. According to linear perturbation theory, a highly elongated bar breaks up gravitationally into fragments, with separations comparable to the wavelength of the most unstable linear perturbation, which corresponds to $\sim 10^2 \text{ AU}$ at $\sim 10^{12} \text{ cm}^{-3}$. The typical masses of the fragments are in the substellar regime. Some of the fragments could be ejected out of the system in the course of dynamical interaction (see also Bate et al. 2002). Those ejected may become isolated brown dwarfs (Reipurth & Clarke 2001) and perhaps even free-floating massive planets. Interestingly, the cloud parameters derived by Ciolek & Basu (2000) for the well-studied starless core L1544 put the cloud in the bar fragmentation category. Therefore, L1544 appears to be a progenitor of a binary or small multiple star system of the common envelope type.

When the initial cloud mass in the central plateau region is comparable to the thermal Jeans mass (e.g., $r_0 \lesssim 15\pi$ for $n \sim 2$ and $\omega \sim 0.1$), the bar mode does not grow much during the isothermal collapse, and it is difficult for the (relatively short) bar to break up into fragments (*disk fragmentation*). In this case, the central region evolves into a rapidly rotating disk whose size depends on the rate of initial rotation. The interaction of the central disk with the bar generates complex structures in the disk where a secondary bar mode is excited by rotational instability if $\beta \gtrsim 0.3$. Typically, the size of centrifugal radius is of the order of 10 AU. When the disk fragments into blobs, the separations of the blobs should be of the same order of the disk radius. This case may be responsible for the formation of binary stars with a separation smaller than 10^2 AU . This case would be related to the common disk system of Looney et al. (2000).

As mentioned in § 2, we did not consider angular momentum transfer in the vertical direction, which can brake the cloud rotation efficiently during the relatively long magnetically subcritical phase of evolution (Nakano & Tademaru 1972; Basu & Mouschovias 1994). Magnetic braking is thought to be responsible for the low rates of rotation observed in dense cores (Goodman et al. 1993) and adopted in this paper. Once the central region of the cloud becomes supercritical, the peak density increases in a runaway fashion, leaving little time for the magnetic braking to operate efficiently (Basu & Mouschovias 1994). We therefore expect the formation of separate cores, which occurs in the runaway collapse phase, to be little affected by magnetic braking. After a bar or a disk becomes dense enough to be opaque to dust emission, it can be supported

by thermal pressure for a time long compared to the local dynamic time, and magnetic braking can in principle become efficient again (Krasnopolsky & Konigl 2002). However, at such high densities, magnetic fields start to decouple from matter (Nishi, Nakano, & Umebayashi 1991), which could render the braking inefficient. We will postpone a detailed treatment of the magnetic braking including the effects of decoupling to a future work.

6. CONCLUSION

In this paper, we have followed the early phases of cloud fragmentation in magnetic clouds, using a two-dimensional MHD code based on the thin-disk approximation. At the end of our calculations, we obtained dense, discrete fragments out of initially axisymmetric clouds perturbed by an $m = 2$ mode of modest fractional amplitude $A = 0.05$. The masses of the fragments are still small, on the order of $10^{-2} - 10^{-1} M_{\odot}$. We expect the fragments to grow to stellar masses, by merging and further accretion, except perhaps those ejected dynamically out of the system soon after the fragmentation. The masses of those ejected may remain frozen in the substellar regime.

We found three types of fragmentation in magnetic clouds. They are (1) a cloud breaking up during the isothermal phase of cloud evolution into separate cores, each of which collapses more or less independently into a star/stellar system (panels [b] and [c] of Fig. 7), (2) a core collapsing into a needle-like, opaque “first bar”, which breaks up into several fragments (Fig. 8), and (3) a rapidly rotating, opaque “first disk” producing self-gravitating blobs, which may survive to become seeds of relatively close binary and multiple systems (Figs. 9 and 10). The fragments in the above cases share, respectively, a common cloud, common core, and common disk. They correspond loosely to the empirical classification of independent envelope, common envelope and common disk systems for the youngest, embedded binary and multiple systems. Much work is needed to firm up this connection.

In the near future, we plan to extend our numerical simulations beyond the initial fragmentation to the protostellar accretion phase, to determine the physical properties of the binary and multiple systems formed in magnetic clouds, such as their eccentricity, mass ratio, and orbital period. In a longer run, we hope to generalize the calculations to 3D, which will allow for a detailed study of magnetic braking, which may have a profound impact on the final orbits of the formed stellar system.

Numerical computations in this work were carried out at the Yukawa Institute Computer Facilities, Kyoto University. F.N. gratefully acknowledges the support of the JSPS Postdoctoral Fellowships for Research Abroad, and Z.Y.L. is supported in part by NASA.

REFERENCES

- Alves, J. F., Lada, C., Lada, E., Lombardi, M., & Bergin, E. A. in *The Origins of Stars and Planets: The VLT View*, ed. J. F. Alves & M. J. McCaughrean (Springer), p. 37
- André, P., Ward-Thompson, D., & Barsony, M. 2000, in *Protostars and Planets IV*, ed. V. Mannings, A. P. Boss, & S. S. Russell (Tucson:University of Arizona Press), p. 59
- Bastien, P. 1983, *A&A*, 119, 109
- Basu, S. 1997, *ApJ*, 485, 240
- Basu, S. 2000, *ApJ*, 540, 103
- Basu, S. & Mouschovias, T. Ch. 1994, *ApJ*, 432, 720
- Basu, S. & Mouschovias, T. Ch. 1995, *ApJ*, 453, 271
- Bate, M. R. 1998, *ApJ*, 508, L95
- Bate, M. R. & Burkert, A. 1997, *MNRAS*, 288, 1060
- Bate, M. R., Bonnell, I. A., & Bromm, V. 2002, *MNRAS*, 332, L65

- Beichman, C. A., Myers, P. C., Emerson, J. P., Harris, S., Mathieu, R., Benson, P. J., & Jennings, R. E. 1986, *ApJ*, 307, 337
- Benz, W. 1984, *A&A*, 139, 378
- Black, D. C. & Scott, E. H. 1982, *ApJ*, 263, 696
- Bodenheimer, P., Burkert, A., Klein, R. I., & Boss, A. P. 2000, in *Protostars and Planets IV*, ed. V. Mannings, A. P. Boss, & S. S. Russell (Tucson:University of Arizona Press), p. 675
- Bonnell, I. 1995, *MNRAS*, 269, 837
- Bonnell, I. & Bastien, P. 1991, *ApJ*, 374, 610
- Boss, A. P. 1993, *ApJ*, 410, 157
- Boss, A. P. 2000, *ApJ*, 545, L61
- Boss, A. P. 2001, *ApJ*, 551, L167
- Boss, A. P. 2002, *ApJ*, 568, 743
- Bouvier, J., Rigaut, F., & Nadeau, D. 1997, *A&A*, 326, 1023
- Brandner, W. & Koehler, R. 1998, *ApJ*, 499, L79
- Brandner, W., Alcalá, J. M., Kunkel, M., Moneti, A. & Zinnecker, H. 1996, *A&A*, 307, 121
- Burkert, A., Bate, M. R., & Bodenheimer, P. 1997, *MNRAS*, 289, 497
- Ciolek, G. E. & Basu, S. 2000, *ApJ*, 529, 925
- Ciolek, G. E. & Mouschovias, T. Ch. 1993, *ApJ*, 418, 774
- Crutcher, R. M. 1999, *ApJ*, 520, 706
- Crutcher, R. M., Mouschovias, T. Ch., Troland, T. H., & Ciolek, G. E. 1994, *ApJ*, 427, 839
- Dorfi, E. 1982, *A&A*, 114, 151
- Duquennoy, A. & Mayor, M. 1991, *A&A*, 248, 485
- Durisen, R. H., Gingold, R. A., Tohline, J. E., & Boss, A. P. 1986, *ApJ*, 305, 281
- Evans, N. J. II, Rawlings, J. M. C., Shirley, Y. L., & Mundy, L. G. 2001, *ApJ*, 557, 193
- Fischer, D. A. & Marcy, G. W. 1992, *ApJ*, 396, 178
- Fiedler, R. A. & Mouschovias, T. Ch. 1993, *ApJ*, 415, 680
- Fuller, G. A., Ladd, E. F., & Hodapp, K.-W. 1996, *ApJ*, 463, L97
- Galli, D., Shu, F. H., Laughlin, G., & Lizano, S. 2001, *ApJ*, 551, 367
- Ghez, A. M., McCarthy, D. W., Patience, J. L., & Beck, T. L. 1997, *ApJ*, 481, 378
- Goodman, A., Benson, P., Fuller, G., & Myers, P. 1993, *ApJ*, 406, 528
- Goodwin, S. P., Ward-Thompson, D., & Whitworth, A. P. 2002, *MNRAS*, 330, 769
- Indebetouw, R. & Zweibel, E. G. 2000, *ApJ*, 532, 361
- Jones, C. E., Basu, S., & Dubinski, J. 2001, *ApJ*, 551, 387
- Kohler, R., Kunkel, M., Leinert, C., & Zinnecker, H. 2000, *A&A*, 356, 541
- Krasnopolsky, R. & Konigl, A. 2002, *ApJ*, 580, 987
- Langer, W. D. 1978, *ApJ*, 225, 95
- Larson, R. B. 1969, *MNRAS*, 145, 271
- Larson, R. B. 1972, *MNRAS*, 156, 437
- Larson, R. B. 1985, *MNRAS*, 214, 379
- Launhardt, R. 2001, in *The Formation of Binary Stars*, IAU Symposium, Vol. 200, eds. H. Zinnecker & R. D. Mathieu (ASP Series: San Francisco), p. 117
- Lee, C. W., Myers, P. C. & Taffala, M. 2001, *ApJS*, 136, 703
- Li, Z.-Y. & Shu, F. H. 1997, *ApJ*, 475, 237
- Li, Z.-Y. 1998, *ApJ*, 497, 850
- Li, Z.-Y. 2001, *ApJ*, 526, 806
- Li, Z.-Y., Shematovich, V., Wiebe, D. & Shustov, B. 2002, *ApJ*, 569, 792
- Li, Z.-Y. & Shu, F. H. 1996, *ApJ*, 472, 211
- Li, Z.-Y. & Nakamura, F. 2002, *ApJ*, 578, 256
- Lin, C. C., Mestel, L., & Shu, F. H. 1965, *ApJ*, 142, 1431
- Leinert, Ch., Zinnecker, H., Weitzel, N., Christou, J., Rigway, S. T., Jameson, R., Hass, M., & Lenzen, R. 1993, *A&A*, 278, 129
- Lizano, S. & Shu, F. H. 1989, *ApJ*, 342, 834
- Looney, L. W., Mundy, L. G. & Welch, W. J. 2000, *ApJ*, 529, 477
- Looney, L. W., Mundy, L. G. & Welch, W. J. 1997, *ApJ*, 484, L157
- Mathieu, R. D. 1994, *ARA&A*, 32, 465
- Mathieu, R. D., Ghez, A. M., Jensen, E. N., & Simon, M. in *Protostars and Planets IV*, ed. V. Mannings, A. P. Boss, & S. S. Russell (Tucson:University of Arizona Press), p. 703
- Matsumoto, T., Hanawa, T., & Nakamura, F. 1997, *ApJ*, 478, 569
- Matsumoto, T., & Hanawa, T. 1999, *ApJ*, 521, 659
- Matsumoto, T., & Hanawa, T. 2002, submitted to *ApJ*
- Mestel, L. & Spitzer, L. Jr. 1956, *MNRAS*, 116, 503
- Motte, F., Andre, P., & Neri, R. 1998, *A&A*, 336, 150
- Mouschovias, T. Ch. & Morton, S. A. 1991, *ApJ*, 371, 296
- Moriarty-Schieven, G. H., Powers, J. A., Butner, H. M., Wannier, P. G. & Keene, J. 2000, *ApJ*, 533, L143
- Mouschovias, T. Ch. & Ciolek, G. 1999, in *The Origins of Stars and Planetary Systems*, ed. C. Lada & N. Kylafis (Kluwer), p. 305
- Myers, P. C. 1999, in *The Origins of Stars and Planetary Systems*, ed. C. Lada & N. Kylafis (Kluwer), p. 67
- Myers, P. C., Fuller, G. A., Goodman, A. A., & Benson, P. J. 1991, *ApJ*, 376, 561
- Nakamura, F., Hanawa, T., & Nakano, T. 1993, *PASJ*, 45, 551
- Nakamura, F., Hanawa, T., & Nakano, T. 1995, *ApJ*, 444, 770
- Nakamura, F. & Hanawa, T. 1997, *ApJ*, 480, 701
- Nakamura, F., Matsumoto, T., Hanawa, T., & Tomisaka, K. 1999, *ApJ*, 510, 274
- Nakamura, F. & Li, Z.-Y. 2002, *ApJ*, 566, L101
- Nakano, T. 1979, *PASJ*, 31, 697
- Nakano, T. & Tadamaru, E. 1972, *ApJ*, 173, 87
- Nakano, T., Nishi, R., & Umebayashi, T. 2002, *ApJ*, 573, 199
- Nishi, R., Nakano, T., & Umebayashi, T. 1991, *ApJ*, 368, 181
- Padgett, D. L., Strom, S. E., Ghez, A. M. 1997, *ApJ*, 477, 705
- Prosser, C. F., Stauffer, J. R., Hartmann, L., Soderblom, D. R., Jones, B. F., Werner, M. W., & McCaughrean, M. J. 1994, *ApJ*, 421, 517
- Phillips, G. J. 1986, *MNRAS*, 221, 571
- Phillips, G. J. 1986, *MNRAS*, 222, 111
- Rodriguez, L. F., D'Alessio, P., Wilner, D. J., Ho, P. T. P., Torrelles, J. M., Curiel, S., Gomez, Y., Lizano, S., Pedlar, A. Canto, J., & Raga, A. C. 1998, *Nature*, 395, 355
- Reipurth, B., & Clarke, C. 2001, *ApJ*, 122, 432
- Reipurth, B., Rodriguez, L. F., Anglada, G. & Bally, J. 2002, *AJ*, 124, 1045
- Ryden, B. S. 1996, *ApJ*, 471, 822
- Saigo, K. & Hanawa, T. 1998, *ApJ*, 493, 342
- Stehle, R. & Spruit, H. C. 2001, *MNRAS*, 323, 587
- Shu, F. H., Allen, A., Shang, H., Ostriker, E., & Li, Z.-Y. 1999, in *The Origins of Stars and Planetary Systems*, ed. C. Lada & N. Kylafis (Kluwer) p. 540
- Shu, F. H. & Li, Z.-Y. 1997, *ApJ*, 475, 251
- Shu, F. H., Adams, F. C., & Lizano, S. 1997, *ARA&A*, 25, 23
- Sigalotti, L. Di G. & Klapp, J. 2001 *A&A*, 378, 165
- Terebey, S. & Padgett, D. L. 1997, in *Herbig-Haro Flows and the Birth of Stars*, IAU Symposium No. 182, eds. Bo. Reipurth and C. Bertout (Kluwer), p. 507
- Tomisaka, K., Ikeuchi, S., & Nakamura, T. 1988, *ApJ*, 335, 239
- Tohline, J. E. 2002, *ARA&A*, 40, 349
- Tsuribe, T. & Inutsuka, S. 1999, *ApJ*, 523, 155
- Ward-Thompson, D., Motte, F. & André, P. 1999, *MNRAS*, 305, 143
- Whitworth, A., Chapman, S. J., Bhattal, A. S., Disney, M. J., Pongracic, H. & Turner, J. A., 1995, *MNRAS*, 277, 727
- Williams, J. P. & Myers, P. C. 2000, *ApJ*, 537, 891
- Wootten, A. 1989, *ApJ*, 337, 858
- White, R. J. & Ghez, A. M. 2000, *ApJ*, 556, 265
- Young, C. H., Shirley, Y. L., Evans, N. J. II, & Rawlings, J. M. C. 2002, *ApJ*, in press (astro-ph/0210182)

TABLE 1
PARAMETERS OF MODELS

r_0	n	ω	Γ_0	perturbation	A	display
10π	2	0.0	1.5	$m = 2$	0.05	Fig. 1 (standard model)
10π	2	0.0	1.25	$m = 2$	0.05	Fig. 4a
10π	2	0.1	1.5	$m = 2$	0.05	Fig. 5
15π	2	0.0	1.5	$m = 2$	0.05	Fig. 4b
15π	2	0.2	1.5	$m = 2$	0.05	Fig. 8 (bar fragmentation)
5π	2	0.1	1.5	$m = 2$	0.05	Figs. 9, 10 (disk fragmentation)
5π	4	0.0	1.5	$m = 2$	0.05	Fig. 4c
5π	4	0.1	1.5	$m = 2$	0.05	Fig. 7a
5π	4	0.2	1.5	$m = 2$	0.05	Figs. 7b,c (separate core formation)

Note. — All models are computed on an initial grid of 512×512 in the disk (x - y) plane. For the standard model shown in Fig. 1, the grid number is increased to 1024×1024 for each level of refinement.

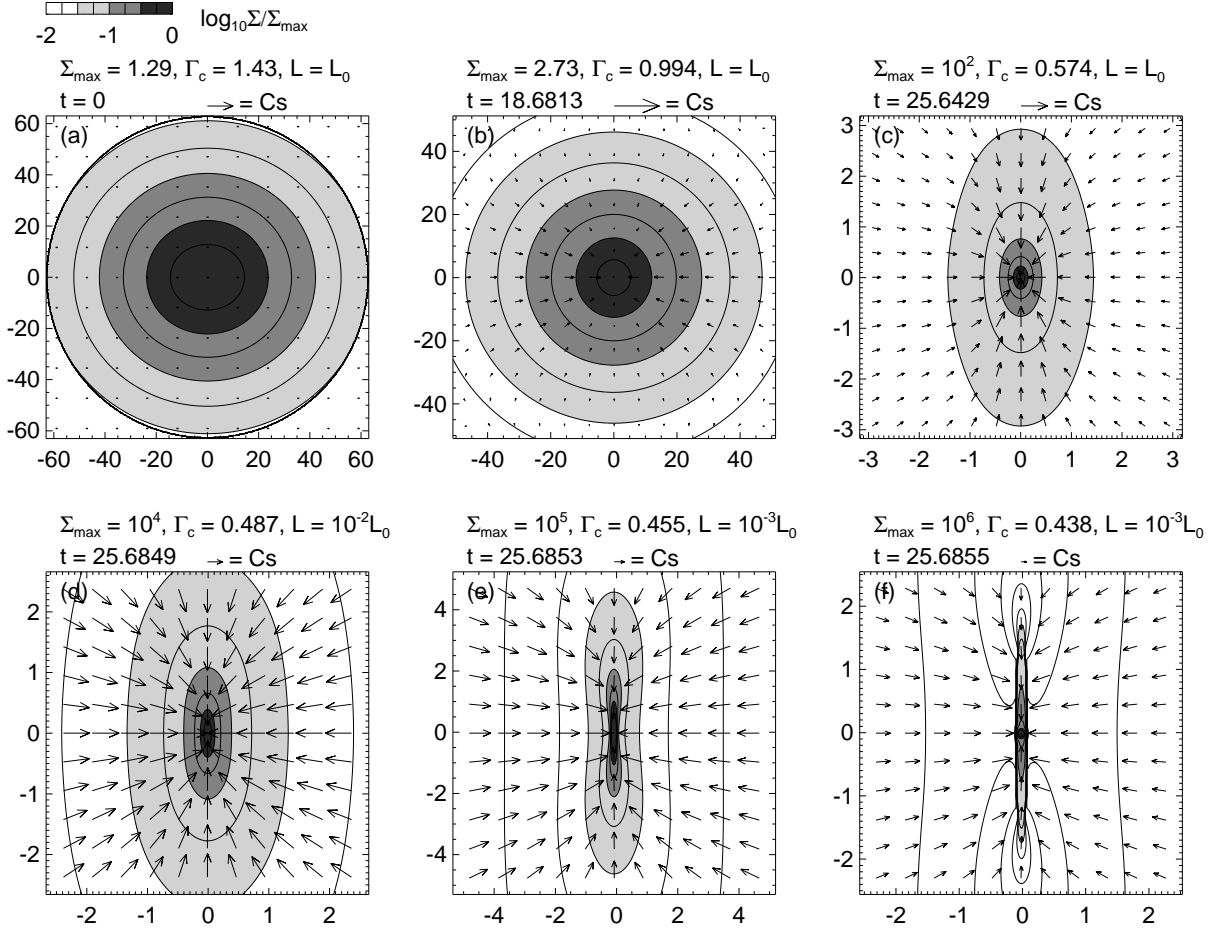


FIG. 1.— Snapshots of the surface density distribution and velocity field for the non-rotating cloud perturbed by an $m = 2$ mode of fractional amplitude $A = 0.05$ at six dimensionless times: (a) $t=0$, (b) 18.6813, (c) 25.6429, (d) 25.6849, (e) 25.6853, and (f) 25.6855. The model cloud has a set of “standard” parameters of $(r_0, n, \omega, \Gamma_0) = (10\pi, 2, 0, 1.5)$. Panel (a) shows the initial state. In panels (b) through (f), only the central regions are shown. The contour curves in each panel are for the surface density normalized by Σ_{\max} , whose value is given above each panel. Also given are the flux-to-mass ratio (Γ_c) at the density peak, and length unit for each panel. The arrows are velocity vectors normalized by the effective isothermal sound speed c_s (without magnetic contribution), whose magnitude is indicated above each panel. Note that in panel (a) the added perturbation lowers the flux-to-mass ratio $\Gamma = 1.43$ from the reference value $\Gamma_0 = 1.5$ by 5%, corresponding to the fractional amplitude of the perturbation. For dimensional units, see § 2.

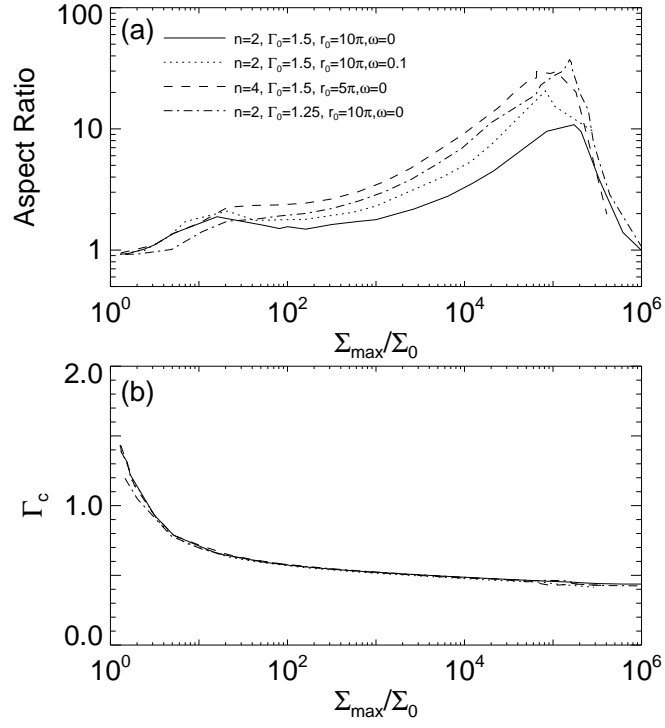


FIG. 2.— Evolution of (a) the aspect ratio of the highest density region with surface density above $10^{-1/2}\Sigma_{\max}$, and (b) the flux-to-mass ratio Γ_c at the surface density maximum. Solid curves are for the standard model with $n = 2$, $\Gamma_0 = 1.5$, $r_0 = 5\pi$, and $\omega = 0$.

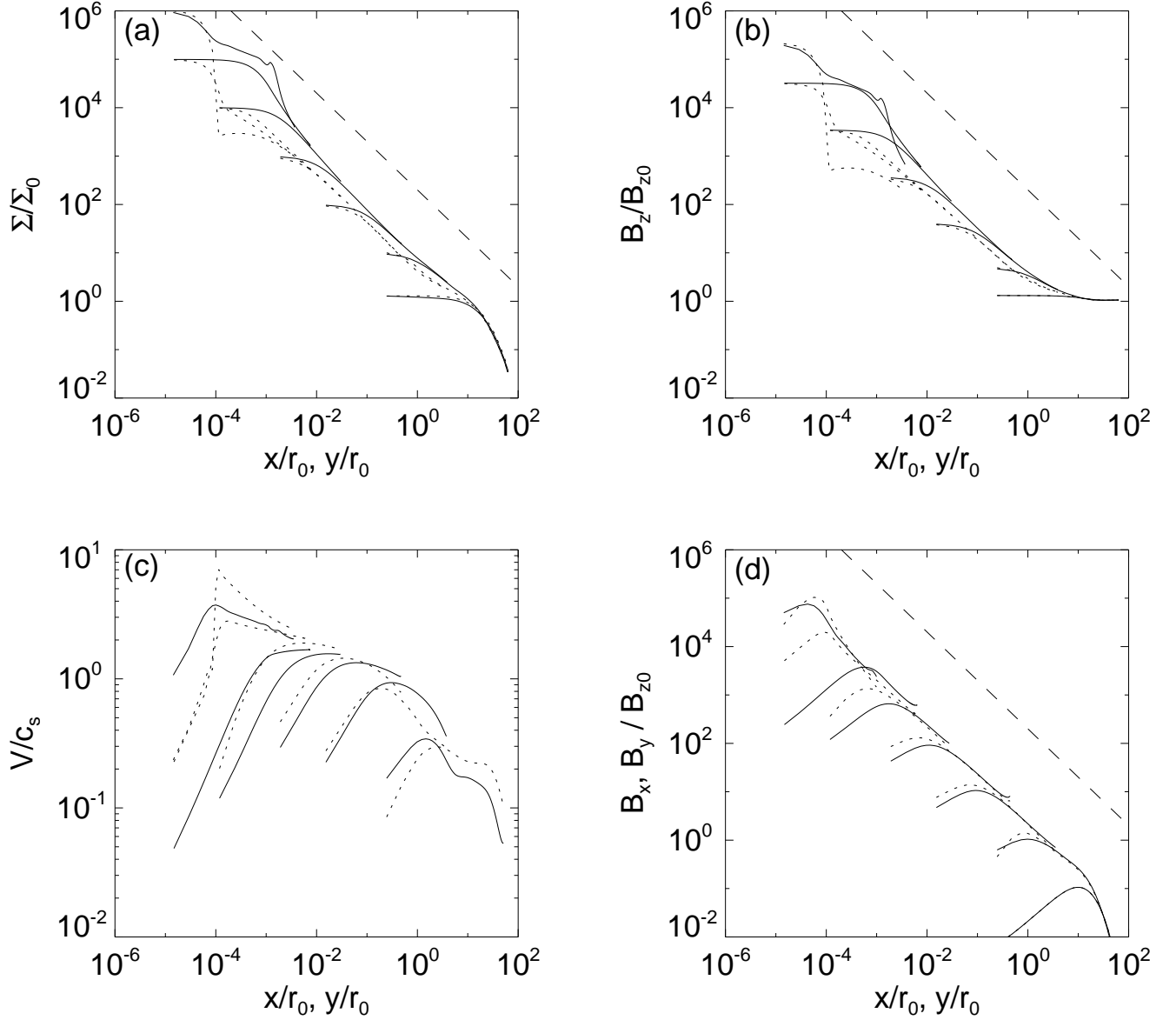


FIG. 3.— Distributions of surface density Σ , infall speed V , and the vertical magnetic field strength B_z , and the two components of magnetic field in the disk plane (B_x and B_y) along the major (solid lines) and minor (dotted lines) axes of the standard model shown in Fig. 1, at seven different times. Note that before the breakdown of isothermal equation of state the surface density and the strength of each magnetic field component approach a power-law distribution of $\propto d^{-1}$ (plotted as a dashed line in panels [a], [b], and [d], with d denoting the distance from the center), and the infall speed is more or less constant. This self-similar behavior of isothermal collapse is explored further in §3.4. In panels (b) and (d), the solid and dotted lines coincide with each other at the initial state because of the initial axisymmetric magnetic configuration. In panel (c), the initial infall speed is equal to zero owing to the static initial condition and accordingly not depicted.

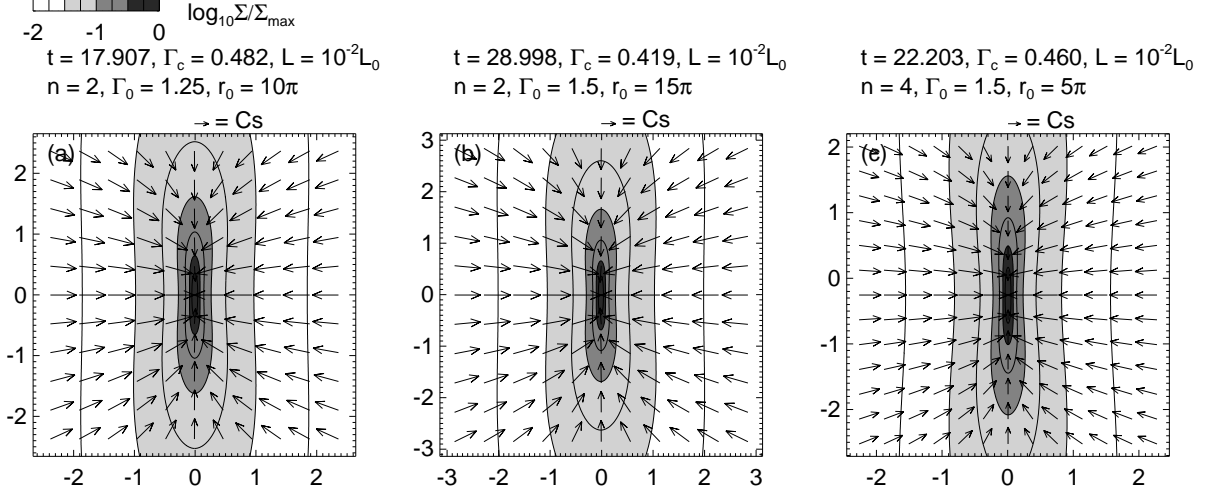


FIG. 4.— Snapshots of the surface density distribution and velocity field at the time when $\Sigma_{\max} = 10^4$ for the nonrotating models with different model parameters. Panel (a): the model with a weaker magnetic field, $(r_0, n, \omega, \Gamma_0, A) = (10\pi, 2, 0, \underline{1.25}, 0.05)$, showing that decreasing field strength promotes bar growth. Panel (b): the model with a larger r_0 , $(r_0, n, \omega, \Gamma_0, A) = (\underline{15\pi}, 2, 0, 1.5, 0.05)$, showing the positive effect of the initial cloud mass on the bar growth. Panel (c): the model with a larger n and a smaller r_0 , $(r_0, n, \omega, \Gamma_0, A) = (5\pi, \underline{4}, 0, 1.5, 0.05)$, showing the positive effect of a flat density distribution. These panels should be compared with panel (d) of Fig. 1. The contours, arrows and notations have the same meaning as in Fig. 1. The parameters having different values from those of Fig. 1 are underlined.

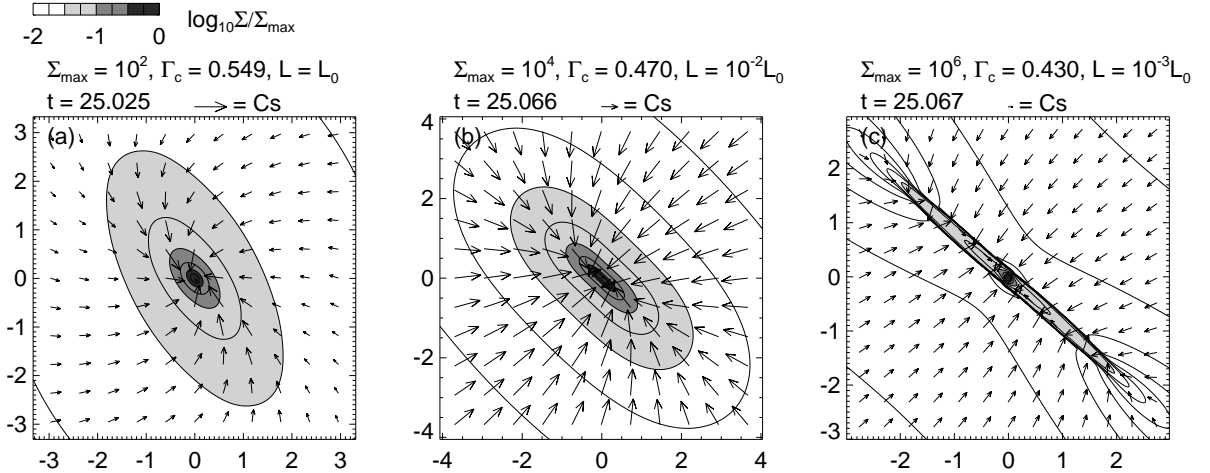


FIG. 5.— Snapshots of the surface density distribution and velocity field of the slowly-rotating model with $(r_0, n, \omega, \Gamma_0, A) = (10\pi, 2, \underline{0.1}, 1.5, 0.05)$ at three different stages: (a) $t = 25.025$, (b) $t = 25.066$, and (c) $t = 25.067$. The contours, arrows and notations have the same meaning as in Fig. 1. The parameters having different values from those of Fig. 1 are underlined. Comparison with panels (c) through (e) of Fig. 1 points to a positive effect of the slow rotation on the bar growth.

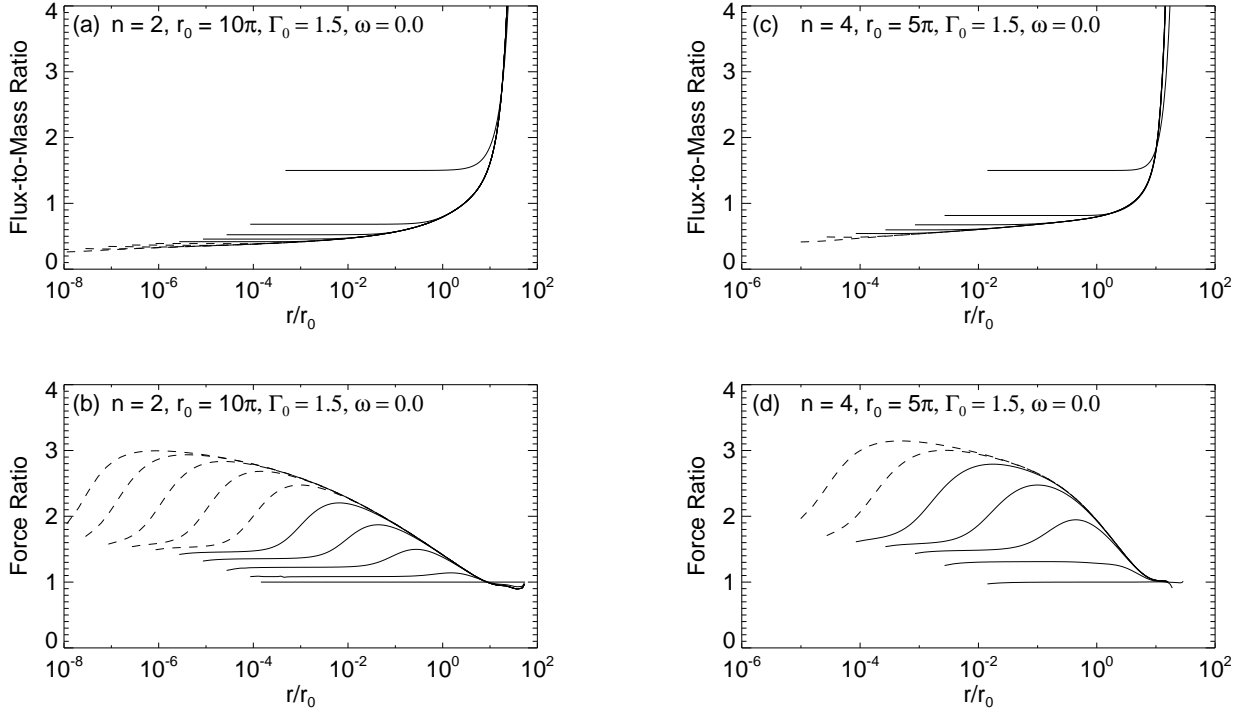


FIG. 6.— Axisymmetric evolution of two clouds without perturbations. Plotted are (a) the flux-to-mass ratio and (b) the force ratio for a centrally-condensed model with the standard set of cloud parameters $(r_0, n, \omega, \Gamma_0) = (10\pi, 2, 0, 1.5)$, and (c) the flux-to-mass ratio and (d) the force ratio for a less centrally-condensed model with $(r_0, n, \omega, \Gamma_0) = (5\pi, 4, 0, 1.5)$, at times when $\Sigma_c = 1.2(t=0), 10, 10^2, 10^3, \dots$. The force ratio is defined as the ratio of the effective gravity ($F_{g,\text{eff}}$) to the effective pressure force ($F_{P,\text{eff}}$), where $F_{g,\text{eff}} = F_{\text{grav}} + F_{\text{ten}}$ and $F_{P,\text{eff}} = F_{\text{gas}} + F_B$. In these one-dimensional calculations, we do not stiffen the isothermal equation of state even when the surface density exceeds the critical value of $\Sigma_{\text{cr}} = 1.9 \times 10^4$. In all panels, we show the distributions at the times when $\Sigma_c > \Sigma_{\text{cr}}$ separately with dashed lines.

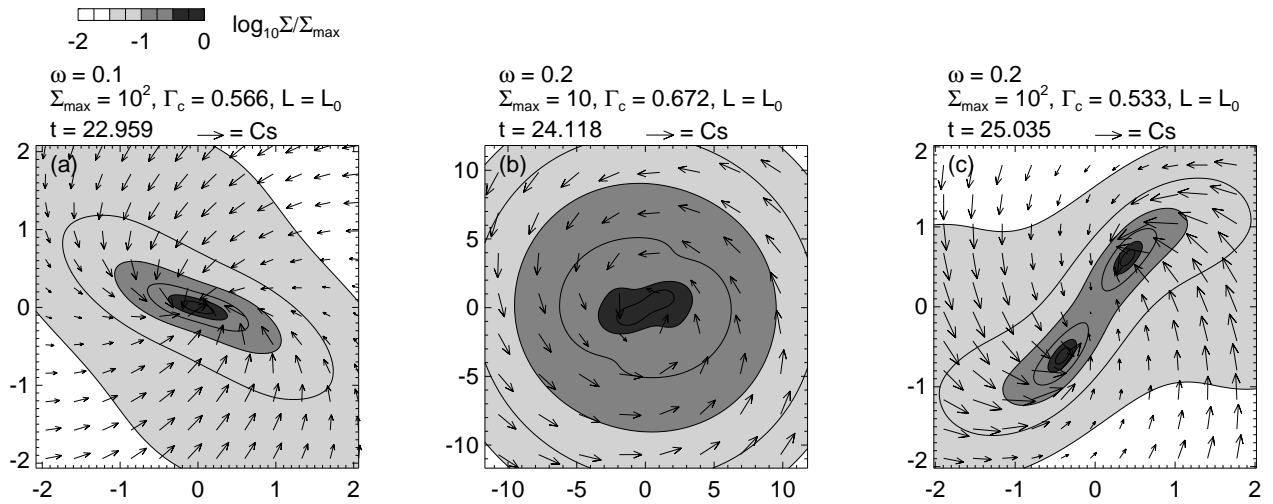


FIG. 7.— Snapshots of the surface density distribution and velocity field of two models (a) with $(r_0, n, \omega, \Gamma_0, A) = (5\pi, 4, 0.1, 1.5, 0.05)$, and (b) and (c) with $(r_0, n, \omega, \Gamma_0, A) = (5\pi, 4, 0.2, 1.5, 0.05)$. The contours, arrows and notations have the same meaning as in Fig. 1. The parameters having different values from those of Fig. 1 are underlined. In the more rapidly rotating model, the initially-imposed $m = 2$ mode evolves into a long bar, which breaks up into two distinct cores (panel c).

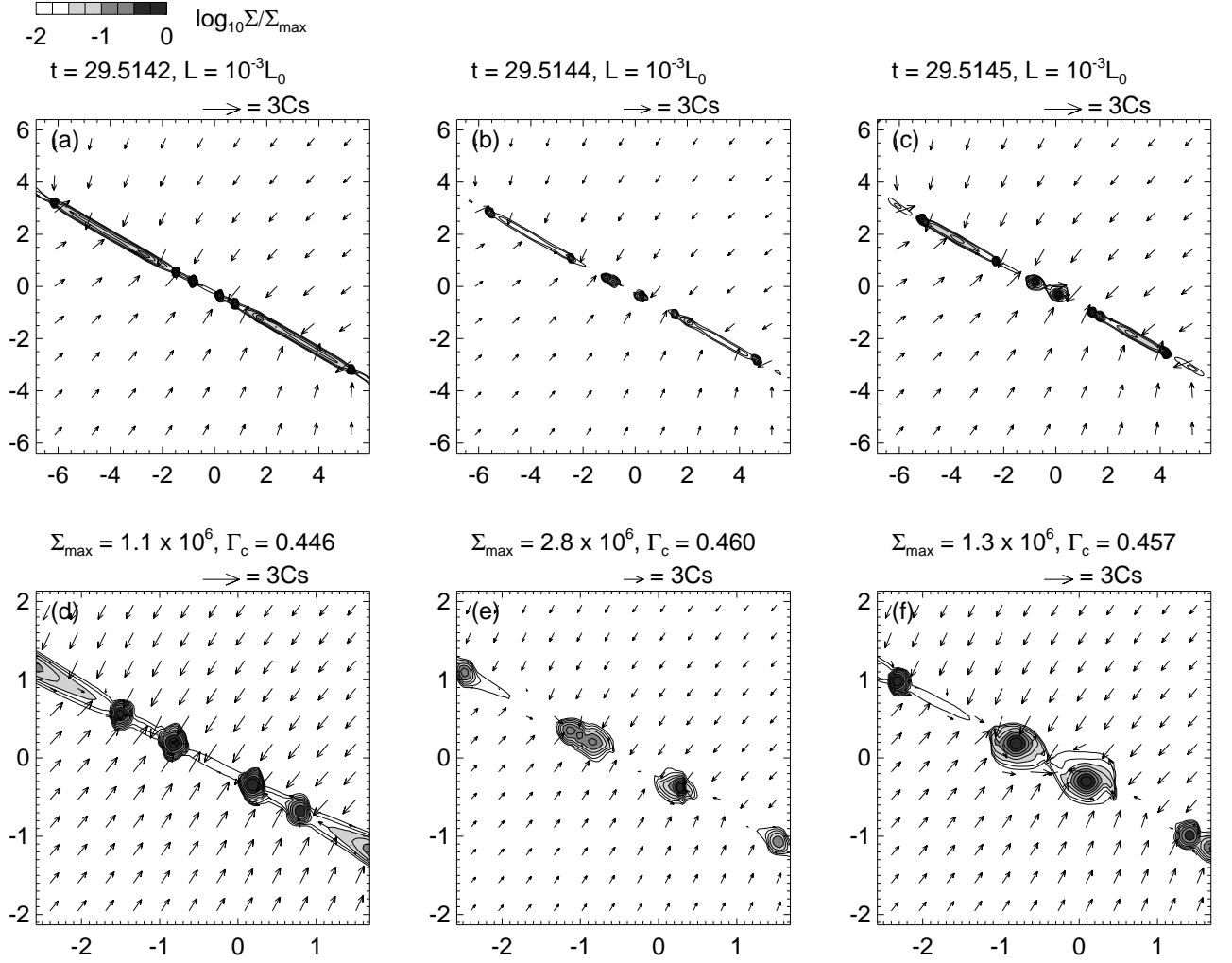


FIG. 8.— Snapshots of the surface density distribution and velocity field of the model with $(r_0, n, \omega, \Gamma_0, A) = (\underline{15\pi}, 2, \underline{0.2}, 1.5, 0.05)$ at three different times: (a) $t = 29.5142$, (b) $t = 29.5144$, and (c) $t = 29.5145$. Panels (d) through (f) show the enlargement of the central region of panels (a) through (c), respectively. The contours, arrows and notations have the same meaning as in Fig. 1. The parameters having different values from those of Fig. 1 are underlined. In this model, the aspect ratio of the first bar becomes very large and the fragmentation starts near the center and at the ends (panel a). Subsequent fragmentation occurs successively in the high density central region, and seemingly propagates towards the ends (panel b). At the same time, the central fragments merge together to form more massive fragments (panel b). This process is repeated at the time shown in panel (c).

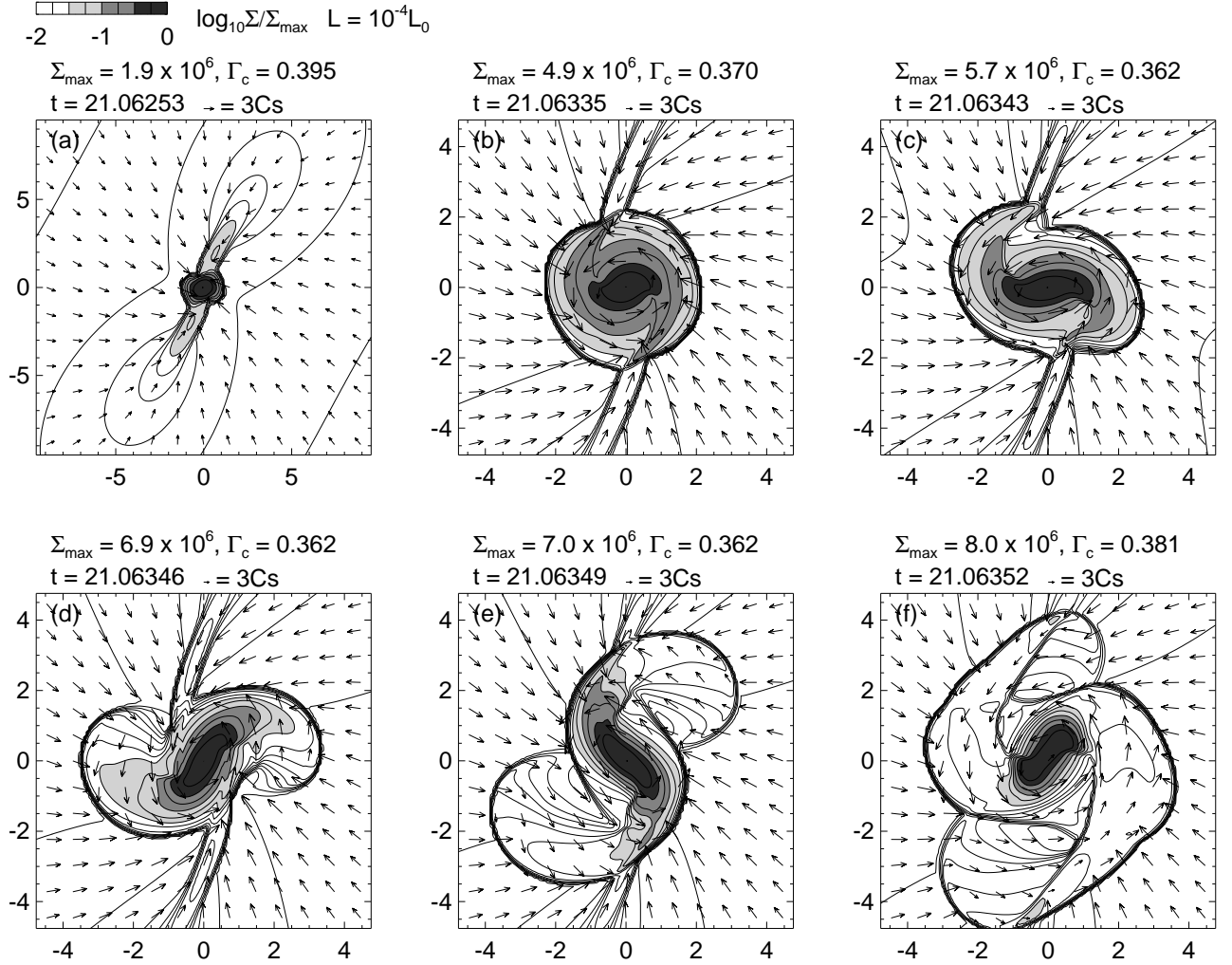


FIG. 9.— Snapshots of the surface density distribution and velocity field of the model with $(r_0, n, \omega, \Gamma_0, A) = (5\pi, 2, \underline{0.1}, 1.5, 0.05)$ at six different times. The contours, arrows and notations have the same meaning as in Fig. 1. The parameters having different values from those of Fig. 1 are underlined. As the infall along the major axis becomes significant, the truly first core is formed at the center, which evolves into a rapidly rotating disk (panel a). In the rotating disk, an $m = 2$ mode develops, which interacts with the inflows along the first bar (panels b and c), generating shock waves in several places (panels d and e). The disk fragments into several blobs due to complex shock interaction (panels e and f).

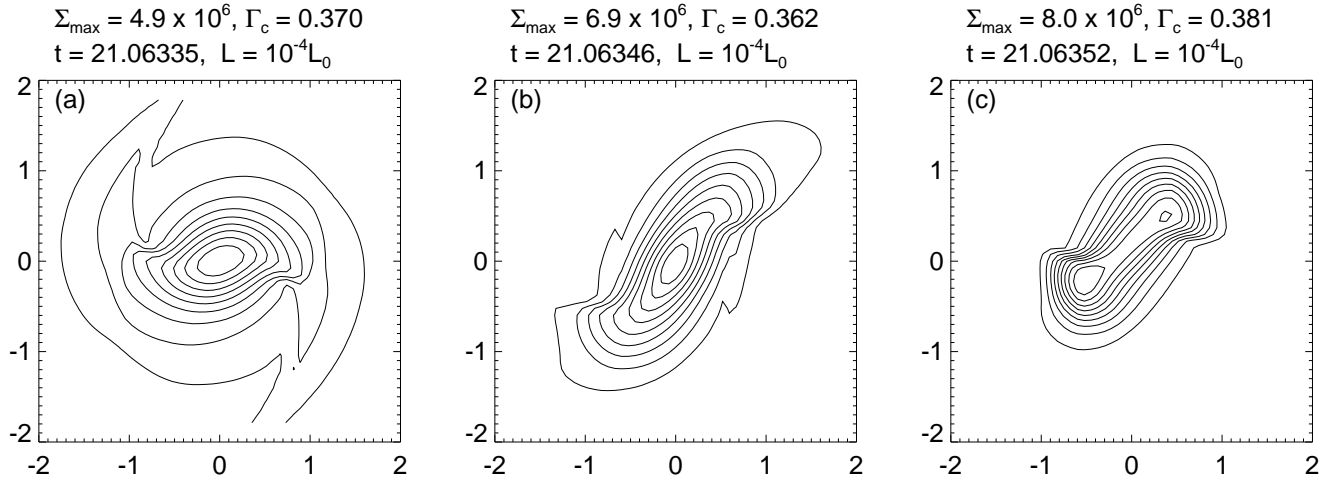


FIG. 10.— Surface density distributions of the central rotating disk for the model with $(r_0, n, \omega, \Gamma_0, A) = (5\pi, 2, 0.1, 1.5, 0.05)$ at three different times. Panels (a), (b) and (c) are at the same times as panels (b), (d), and (f) of Fig. 9. The surface density contours are linear in scale, plotted at levels of 0.1, 0.2, ..., 0.9 of the maximum, Σ_{\max} . At the time shown in panel (c), the bar breaks up into two blobs, which appear to be self-gravitating.